SECTION 26

MICROWAVE BRIGHTNESS TEMPERATURE OF A WINDBLOWN SEA

by

Forrest G. Hall
NASA Manned Spacecraft Center
Houston, Texas

INTRODUCTION

The microwave brightness temperature of the windblown ocean surface has been a problem of interest for several years. The problem simply stated is, how is the microwave electromagnetic radiation emitted and reflected from the ocean surface affected by the wind generated roughness of the water surface (waves and white caps)?

The relevance of this problem lies in the fact that the brightness temperature of a sea surface is dependent upon the roughness of the surface, which in turn depends to some extent on the windspeed at the surface. Thus by measuring the microwave brightness temperature remotely and comparing this result to the actual or kinetic temperature of the sea water, the deviation of these two results can be utilized to remotely measure wind speeds over the world's oceans. The importance of such data to accurate weather prediction is discussed at some length by Moore and Pierson (1970) and Aukland et al. (1970).

The problem has been treated in a fundamental way by Peake (1959) and more recently by Stogryn (1967). Stogryn utilizes some of the notions developed by Peake to develop a specific model for the microwave brightness temperature of the sea as a function of wind speed. His model is based on the Kirchoff approximation for scattering from rough, finitely conducting surfaces. In essence, this approximation assumes that the radius of curvature of each surface wave viewed by the microwave sensor, is not exceeded by the characteristic wavelength of the viewing sensor. For a 19.35 GHz radiometer, the characteristic wavelength c/f, is equal to 1.5 cm; thus as the number of the waves which have radii of curvature exceeding 1.5 cm increases, the accuracy of the Kirchoff approximation decreases.

Undoubtedly many surface features on a windblown sea have radii of curvature less than the characteristic wavelengths of currently operating microwave radiometers (0.8-21 cm). Crests of waves, particularly capillaries, sea spray, white caps and foam will all have some surface features which violate the Kirchoff criteria. The extent to which waves violate this criteria and the effects such a violation will have on the Kirchoff model is not known at this time.

The effects of white caps and sea foam, however, are documented in the experimental work of Williams (1971). His work indicates an extremely high emissivity for foam which cannot be consistent with a Kirchoff model. Thus, it is clear that the portion of the sea surface covered by "white water" must be treated by a different model.

That no model exists which treats the compound sea surface (white water plus clear water) invites the line of investigation discussed in this paper.

In essence the model developed here treats the clear water portion of the surface with the Kirchoff approximation and the white water portion with a model for foam emissivity developed by Droppleman (1970). Although the Kirchoff approximation is employed for the clear water, the approach to the calculation of the brightness temperature is different than the one employed by Peake and Stogryn. As will be seen, the ensuing model produces results which differ in certain respects from Stogryn's model: even for the clear water case. A more drastic deviation in the results of the two models occurs when white water begins to appear on the ocean surface. This result is not surprising and has been documented in the field by several investigators: Nordberg et al. (1970), Hollinger (1971), and Ross et al. (1970).

In addition, but not secondary, to those portions of microwave-sea surface model mentioned above, the atmospheric model plays a vital role in the determination of the microwave brightness temperature. In fact, the sea surface and atmosphere interact as a single unit to produce the total microwave effect. The atmosphere is very "hot" at certain microwave frequencies and as a result this atmospheric radiation reflected by the ocean surface produces a major portion of the change in brightness temperature with increasing surface roughness, especially when little or no white water is present. Thus, it is important to incorporate in the total model an accurate atmospheric radiation model which will specify the radiation intensity of the atmosphere as a function of the radiation frequency and condition of the atmosphere. The model shown here was developed by Paris (1971). Paris' model accounts for the absorbtion and reradiation of microwave electromagnetic radiation from the two major atmospheric contributors, oxygen and water vapor. The inputs to his program are radiosonde data, i.e., pressure, temperature, and relative humidity as a function of altitude. Although this feature of his program provides for the inclusion of actual ground truth data into the model, we do not utilize this feature here; instead we read in hypothetical radiosonde data based on a standard atmosphere. Another important feature of the atmospheric model is its treatment of refractive effects in the atmosphere. This feature is especially important for zenith angles near the horizon.

I would like to acknowledge various members of the Lockheed Electronics Company for their contributions to this effort; Dr. Jack Paris and Dr. Jerry Droppleman for providing coded atmospheric and sea water emissivity subroutines; Mr. Walter Hanby for developing the wave slope generator, incorpora-

tion of the atmospheric and sea water subroutines into the main program and the output routines; finally Mr. Mel Shelton for coding and debugging the main program.

METHOD OF ANALYSIS

In this section we will define the composite model for the ocean surface and outline the computer scheme employed to obtain the brightness temperature based on such a model. Detailed derivations are omitted and only the relevant relationships used will be given.

THE COMPOSITE OCEAN SURFACE MODEL

In our analysis we employ a numerical computer scheme to calculate the total amount of microwave power radiated and reflected into an antenna located an altitude h above a continuous, stationary random surface. This analysis is valid only for those surfaces which are reasonably described by the following mathematical model: A composite stationary random surface consisting of I distinct parts, such that each part is either a specular surface or a slightly rough surface at the characteristic radiometer frequency.

We will assume for our analysis that the surface of a wind blown sea can be usefully approximated by the model described above. More specifically, we will employ a Monte Carlo scheme to computor generate a wind speed dependent, three dimensional sea surface consisting of a composite of two parts: (1) a clear water component, representable by a collection of statistically distributed flat, specular surfaces and (2) a white water component consisting of whitecaps, streaks and foam.

The Clear Water Component

We will assume that the clear water portion of the ocean surface, i.e., that portion not obscured by white caps or foam, can be represented by a collection of plane specular facets, whose surface normals are oriented with respect to the local vertical according to the distribution empirically obtained by Cox and Munk (1954). Cox and Munk discovered experimentally that a good approximation to the distribution $P(\alpha,\varphi)$ of the wave slopes with respect to the zenith angle α and the azimuth angle φ (measured from the crosswind axis) is gaussian and of the form

$$P(\alpha,\varphi) = \frac{1}{2\pi\sigma_c\sigma_u} e^{-\frac{1}{2}\tan^2\alpha\left[\frac{\cos^2\varphi}{\sigma_c^2} + \frac{\sin^2\varphi}{\sigma_u^2}\right]} \qquad (1)$$

where σ_c^2 is the mean square slope, crosswind component and σ_u^2 is the mean square slope, upwind component. Cox and Munk found these components to be linearly related to the wind speed W(m/sec.) in the manner shown below. The value $\alpha = \sqrt{\sigma_u^2}$ is plotted in Figure 1.

$$\sigma_c^2 = 0.003 + 1.92 \times 10^{-3} W$$

$$\sigma_u^2 = 3.16 \times 10^{-3} W \qquad (2)$$

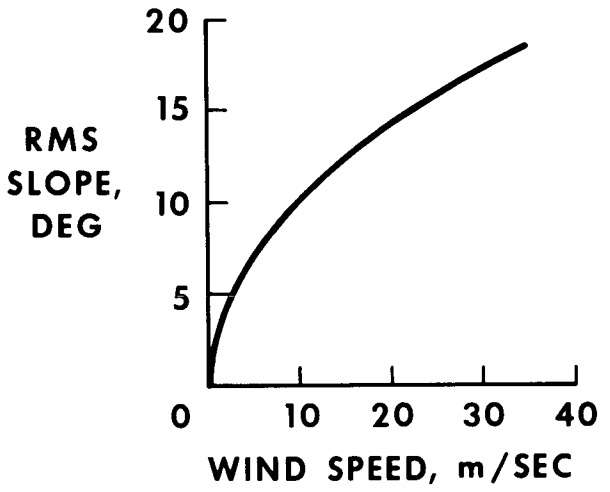

Figure 1.- The rms deviation from the local vertical of the normal to the surface of a wave as a function of wind speed. After Cox and Munk (1954).

In our model then, we develop a MonteCarlo scheme to orient the specular clear water facets, for a given wind speed, according to the distribution of equation (1).

The optical properties of each of these facets are then determined by the Fresnel coefficients and the peculiar geometry which each facet finds itself oriented with respect to the antenna. The dielectric constant for the Fresnel coefficients is calculated using a model developed by Paris (1969).

The White Water Component

Three categories of white water exist on the surface of a heavy sea: whitecaps, spray, and foam. White water makes its appearance when the wind speed increases to the neighborhood of 8 m/sec. Above this speed the percent coverage by white water increases monotonically until the surface is completely obscured around 60 m/sec. (see Neumann and Pierson (1966)). Percent white water coverage as a function of wind speed, has been modeled for wind speeds above 7.5 m/sec. by Cardone (1970). His model agrees roughly with observations by Blanchard (1963). Cardone's results are displayed in Figure 2.

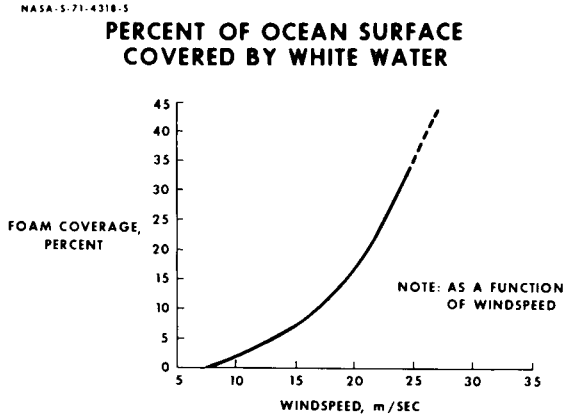

Figure 2.- Percent coverage of the ocean surface as a function of wind speed. After Cardone (1970).

As with wave slopes discussed in the previous section, we employ a Monte Carlo scheme in a computer program to generate white water on the ocean surface. The wind speed is an input to the computer program and the Monte Carlo routine generates an amount of white water specified by Cardone's model.

Once white water has been specified, we use the theoretical model developed by Droppleman to compute the emissivity of the white water patch. For a given electromagnetic frequency, the emissivity in this model is a function of the thickness of the white water patch, the angle at which the patch is oriented with respect to the antenna, and the volumetric ratio of water to air contained in the white water. The emissivity can vary from 0.3 to 1.0 depending on the parameters. The Monte Carlo routine is capable of distributing all of these parameters statistically; however, no data is available for either the thickness distribution or the volumetric ratio distribution. Thus, we choose a thickness and a volumetric ratio to generate an emissivity of about 0.95, depending on the orientation of the foam patch with respect to the antenna. For these values of thickness and volumetric ratio, the emissivity is almost insensitive to geometry so that we allow the surface normals to the foam patches to be gaussianly distributed a'la Cox and Munk. The parameters chosen above are clearly arbitrary. We excuse this on the grounds that to our knowledge no such data presently exists and await the time when such data is available to be used in this model.

APPARENT TEMPERATURE OF THE SEA

At microwave frequencies we are allowed the notion of the apparent temperature of the sea. This number, which characterizes the total amount of microwave power radiated and reflected into a microwave antenna viewing the sea surface, is defined by the relation

$$T_{aj} = \int_G T_{bj}\, G(\beta)\, d\Omega \qquad (3)$$

where T_{aj} is the apparent temperature as seen by the jth polarization mode of the ^{aj} antenna, $G(\beta)$ is the antenna gain function ,and $d\Omega$ is a solid angle element of the gain pattern. We will spend the remainder of this section defining the quantity T_{bj}.

Some rather simple relations emerge as a result of the relation given by eq. (3), and we will use this fortuitous circumstance to build our model. This model differs in approach, if not in principle, from Stogryn's model which is based on Peak's definition of the scattering coefficient. In order to understand eq. (3) more clearly let us consider the physics involved in calculating T_{aj}.

Figure 3 depicts a microwave antenna located at some altitude h* above an ocean surface. The Y axis in the figure is chosen to point in the upwind

* h is assumed to be of a sufficient magnitude to guarantee that the surface is in the far field of the antenna pattern.

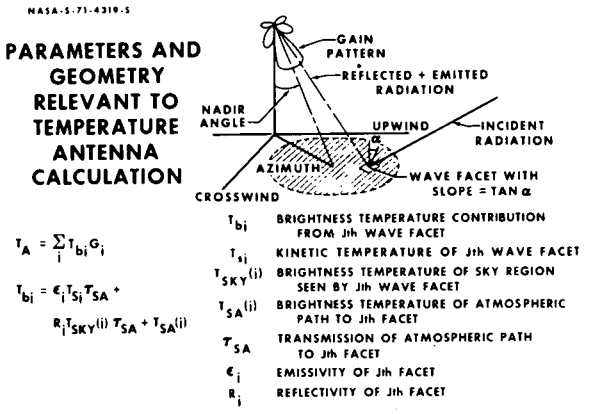

Figure 3.- The Parameters and Geometry relevant to the Antenna Temperature Calculation.

direction and the Z axis along the local normal. The X axis, being right-hand consistent with Y-Z, then points in the crosswind direction.

The angles (θ_o, φ_o) will serve to orient the antenna. We will assume the antenna gain pattern to have a symmetry axis (pointing axis) so that θ_o defines the nadir of the symmetry axis and φ_o defines the azimuth angle with respect to the crosswind X axis. The antenna will then "see" the shaded portion of the ocean surface. We then see from Figure 3 that a wave facet within the shaded area can be located with respect to the symmetry axis by an angle β. β is the angle subtended by the antenna symmetry axis and the dashed line of Figure 3 labeled "reflected + emitted radiation." Each of these wave facets within the shaded area subtends some angle $\Delta\Omega$ in the antenna pattern; thus radiation which is either emitted or reflected from one of these facets will be seen by the antenna. If we partition the gain pattern G into I solid angle increments $\{\Delta\Omega_i\}_{i=1}^{I}$ then I facets will be generated within the shaded area (ignoring antenna side lobes). The integral in equation (3) can thus be transformed into the sum

$$T_{aj} = \sum_{i=1}^{I} T_{bj}^{i} G(\beta_i) \Delta\Omega_i$$

where $\Delta\Omega_i$ is a solid angle increment contained in the gain pattern G and furthermore $\Delta\Omega_i \in \{\Delta\Omega_i\}_{i=1}^{I}$, the partition discussed previously. T_{bj}^{i} is the brightness temperature of the ith facet subtended by $\Delta\Omega_i$.

T_{bj}^{i} is determined by three factors: microwave radiation emitted from the ith facet, microwave radiation emitted from the sky and reflected from the ith facet into the solid angle increment $\Delta\Omega i$ and the radiation attenuated and radiated by the atmosphere contained in $\Delta\Omega_i$. These parts can be represented mathematically by the equation

$$T_{bj}^{i} = \epsilon_j^i T_S^i \alpha_{SA}^i + \rho_j^i T_{SKY}^i \alpha_{SA}^i + T_{SA}^i \qquad (4)$$

where

ϵ_j^i = emissivity of the surface of the ith facet for the jth component of polarization.
T_S^i = kinetic temperature of the surface of ith facet
ρ_j^i = reflectivity of the ith facet for the jth component of polarization
T_{SKY}^i = the sky temperature at the ith facet from that portion of the sky which will be reflected by the ith facet into $\Delta\Omega_i$
α_{SA}^i = fraction of the radiation absorbed by the atmosphere contained in $\Delta\Omega_i$
T_{SA}^i = brightness temperature of the atmosphere contained in $\Delta\Omega_i$

Thus, if we calculate T_{bj}^{i} for each facet, which will be composed either of clear water or white water, and sum the contributions from each facet, then we have calculated the apparent temperature of the sea. As we have seen earlier, the collection of facets must be oriented with slopes corresponding to the distribution found by Cox and Munk. Therefore, a large number of facets must be considered if we are to duplicate their statistics. The volume of calculations arising as a result of this procedure clearly requires the development of a computer program. We have developed such a program at NASA/MSC and will spend the next section describing this program.

THE COMPUTER PROGRAM FOR APPARENT TEMPERATURE OF THE SEA

The logic of the computer program, which calculates the apparent temperature of the sea, follows closely the development outlined so far (see Figure 4 for logic flow chart). First a partition for the gain pattern is selected to conform to the assumed axial symmetry of the pattern and provides a simple iteration scheme for the program. A large part of the program is the iteration logic. This logic selects each $\Delta\Omega_i$ so that a constant area increment ΔA_i is viewed at this surface. This step is needed for statistical purposes. The logic also keeps track of the location of $\Delta\Omega_i$ within the pattern and insures that the entire pattern is exhausted before the program ceases computation. About 20,000 increments are used to divide the pattern. When a particular $\Delta\Omega_i$ has been chosen by the iteration logic, a sequence of steps is initiated which allows calculation of T_{bj}^{i} using equation (4).

The block labeled random foam generator in Figure 4 is a random number generator which decides statistically whether the ith facet is to be white water or clear water. This decision is based on the value for the wind speed and Cardone's model for percent white water coverage (see Figure 2).

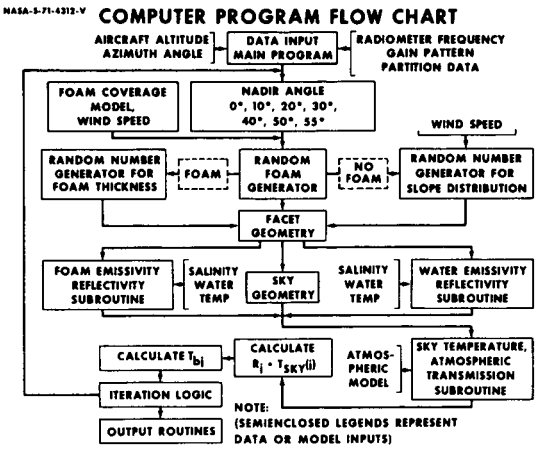

Figure 4.- Computer program flow chart. Random foam generator decides whether left or right side of flow chart is to be executed.

If, for example, the wind speed is 21 m/sec. then for 20 percent of the loops made by the program the sequence (shown in the left side of Figure 4) which calculates T_{bj} for foam is executed.

In the foam sequence, another random number generator, according to yet another distribution function, decides on the thickness of foam to be used. Presently no such data is available and we use a constant thickness as discussed in a previous section in this paper. The geometry of the facet, determined by its location and orientation with respect to the antenna, is then used to calculate the vertically and horizontally polarized emissivities of the facet. These emissivities are calculated using a subroutine developed by Droppleman (1970), also discussed earlier. Once this is accomplished, the program calls a subroutine developed by Paris (1969) which calculates the radiative and absorptive properties of the atmosphere, based on the location of the facet with respect to the antenna and the condition of the atmosphere determined by the radiosonde data input. The program then calculates T_{bj} according to equation (4). This number is stored in the sum register and the program returns to the iteration logic to select another $\Delta\Omega i$.

In case the foam generator decides not to generate a facet covered by white water, then a different sequence is initiated (see right hand side of Figure 4). This sequence contains a random number generator which orients the specular facets according to the distribution of Cox and Munk (1954). Once a facet is oriented with azimuth and zenith angles (φ,α), these angles are used to determine the geometry of the facet with respect to the antenna. This geometry, and the dielectric constant of the sea water (Paris (1969)) are used to determine the horizontal and vertical polarization Fresnel coefficients R_h, R_v. We then assume a randomly polarized incident radiation

(equal intensity in all planes) and use the Fresnel coefficients to calculate the fraction of the incident radiation reflected into the vertical and horizontal polarization planes of the antenna. In terms of the Fresnel coefficients the fraction of incident radiation received by the horizontal mode of the antenna is given by

$$\Pi_v(\theta_p) = \cos^2\theta_p \cdot R_v + \sin^2\theta_p \cdot R_h \qquad (4)$$

The fraction for the vertical polarization mode of the antenna is given by

$$\Pi_h(\theta_p) = \sin^2\theta_p \cdot R_v + \cos^2\theta_p \cdot R_h \qquad (5)$$

where θ_p is the angle subtended by the plane of the surface facet and the antenna horizontal polarization plane.

Once these reflectivities have been calculated then the polarized emissivities are calculated from the coefficients r_v and r_h by

$$\epsilon_j = 1 - \Pi_j \ , \ j = h \text{ or } v \qquad (6)$$

At this point the atmospheric subroutine is called and the sky temperature is calculated along the incident direction defined by the orientation of the specular facet. This subroutine is quite sophisticated. The effects of atmospheric refraction are included, which is quite important at large zenith angles where microwave radiation is strongly refracted. In addition, the program can use radiosonde data taken during the radiometer overflight.

Once the sky temperature T_{sky} (see Figure 3), and the transmission of the atmosphere τ_{sa}, and the brightness temperature T_{SA} of the atmospheric path between the radiometer and the surface facet, have been calculated, equation (4) is evaluated for T_b, the brightness temperature of the facet. A subroutine then retrieves the value for the antenna gain function at this angle β, multiplies this by T_b and adds it to those T_b already calculated. The program is then ready to iterate to another facet.

After the volume of the antenna pattern has been exhausted then the output routines are activated. This output consists of tables and plots of brightness temperature vs. nadir angle for various wind speeds. The program will also print all parameters used in the calculation of T_a: sky temperature vs. zenith angle calculated from radiosonde data: the distribution of surface wave slopes generated by the random number generators: the percent foam coverage generated: a three dimensional wire plot of the antenna pattern.

This general description of the computer program completes the analysis section. We would like now to present some results from this program.

RESULTS

In this section we will present a portion of those results which have so far been obtained from this program. To this date, brightness temperatures versus wind speed data have been generated for each characteristic frequency of all microwave radiometers presently employed on NASA/MSC aircraft. These frequencies are 1.41, 1.42, 4.9, 10.62,10.69, 13.9, 19.35, 22.23, 31.4, 37.0 GHz. As of yet, this model has not been compared to data gathered in a field situation, where for our model we would use an actual gain pattern with radiosonde determined or in situ measured sky temperatures. We will, however, in the first part of this section, compare the results of our model to those results from Stogryn's (1967) model. We will then present curves displaying the increase in brightness temperature with wind speed (wind sensitivity) for winds less than 8 m/sec. (no white water) as a function of radiometer frequency and nadir look angle. Next we will present curves indicating the effects of white water on the brightness temperature. Finally we will examine the wind sensitivity for the 1.4 GHz radiometer at nadir and 55 degrees from nadir for wind speeds above 10 m/sec.

Figure 5 is a sample output from the computer program. These curves are for a 19.35 GHz radiometer viewing a sea surface at 290° K. The curve

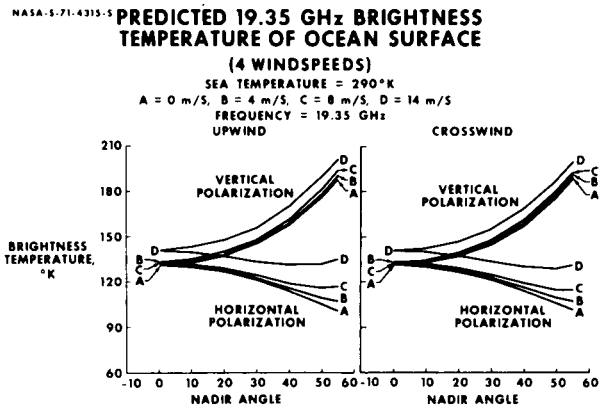

Figure 5.- The predicted brightness temperature of the ocean surface at 19.35 GHz using composite surface model. Aircraft altitude is 1 km.

labeled A is for a calm wind for which the ocean surface is flat. As wind speed increases to 4 meters/sec., curve B is generated. Notice from curve A to curve B that at large nadir look angles the horizontally polarized brightness temperature increases a few degrees Kelvin while the vertically

polarized component increases only slightly. This trend continues until curve D, where a sudden increase from curve C in both the vertically and horizontally polarized brightness temperatures can be observed at all nadir angles. This sudden increase is a result of the onset of significant coverage by white water at 8 m/sec. For the left most curve in this figure, the antenna is pointed directly upwind. In the rightmost curve it is pointed directly crosswind. Some minor differences exist between these two curves. The differences are probably not large enough to capitalize on them experimentally.

Using our model, brightness temperature computations were made at 19.35 GHz and the results compared to those obtained by Stogryn. To effect a better comparison, Stogryn's atmospheric model was substituted for Paris' model. For the horizontally polarized brightness temperature our results are identical to Stogryn's except we predict a slight wind sensitivity (.025 $^{o}K/m\text{-}sec^{-1}$) at nadir. For the vertically polarized case we predict, in contrast to Stogryn's results, a small wind sensitivity at all nadir angles. Thus we do not see the 52° crossover in these curves as predicted by Stogryn. By disabling the foam generator in the computor routine we can see the crossover, but only at windspeeds above 30 m/sec. Such a phenomenon is obscured by the effects of white water.

For the case where no white water exists, we can calculate the increase in brightness temperature with increasing wind speed as a function of nadir look angle. These results are presented in Figure 6. Only the sensitivity for the horizontal polarization mode is plotted. At nadir the wind sensitivity is minimum and increases rapidly beyond 45°. Of the frequencies plotted,

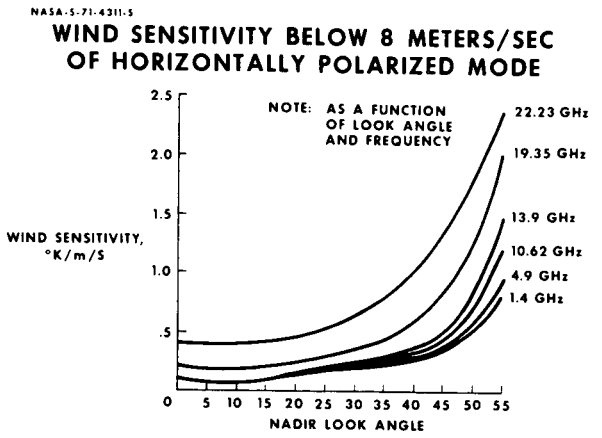

Figure 6.- Increase in brightness temperature with increasing wind speed (wind sensitivity) for wind speeds less than 8 m/sec. (no white water). Aircraft Altitude is 1 km.

the maximum sensitivity is observed for a frequency of 22.23 GHz. This phenomenon will be discussed in the next section. Remember that these sensitivities are for the ocean surface without whitecaps.

In the next figure, figure 7, are displayed the brightness temperature versus lookangle for wind speeds above 10 m/sec. 1.41 GHz was chosen to minimize the effects of clear water roughness. In these plots there is a large increase with wind speed at all nadir angles in both the vertically and horizontally polarized brightness temperature. This is a result of the increasing surface coverage of highly emissive whitecaps and foam.

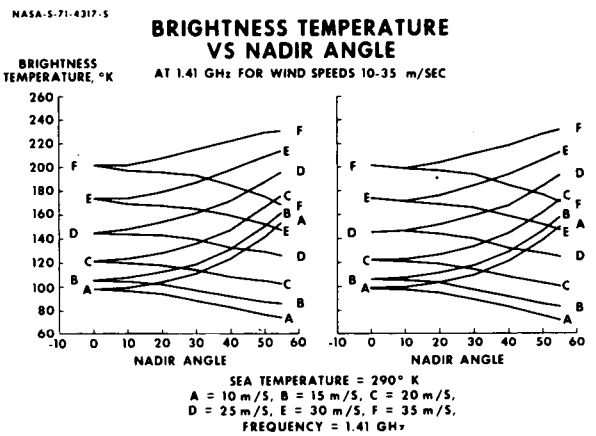

Figure 7.-The predicted brightness temperature increase of the ocean surface at 1.41 GHz using composite surface model. h = 1km.

The data in Figure 7 can be plotted in a different way to reveal a very interesting phenomena. We have done this in Figure 8 where brightness temperature is plotted versus wind speed and percent white water coverage for two nadir look angles. The slope of these curves is thus wind sensitivity or white water coverage sensitivity. For wind speeds less than 20 m/sec., the curve for a nadir angle of 55° has the greatest slope, thus the greatest wind sensitivity; For wind speed above 20 m/sec., however, the nadir pointed radiometer is most wind sensitive.

This result could be of considerable consequence to investigators since data reduction for the nadir pointed radiometer, especially from orbit, is considerably simpler than data reduction at the larger pointing angles. Whether or not this result holds for frequencies other than 1.4 GHz is not known, only because computations at other frequencies for wind speeds above 14m/sec. have not yet been made.

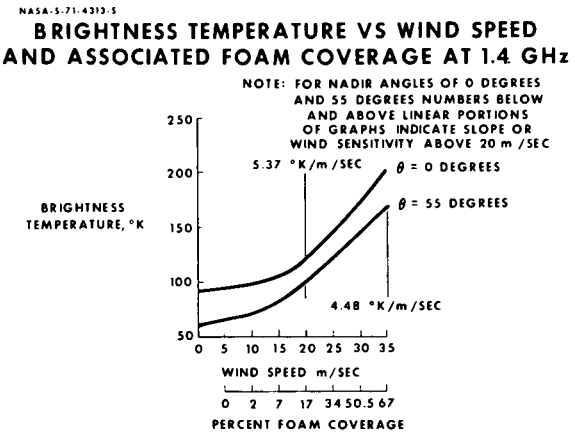

Figure 8.-Brightness temperature versus wind speed and foam coverage at 1.41 GHz for the horizontally polarized mode. h = 1km.

We should reiterate here that our choice to use 1.4 GHz for the initial computations implies no endorsement over other frequencies for wind speed determination.

DISCUSSION

In this section we will address ourselves to a discussion of the deficiencies and merits of the numerical technique and physical models we have employed in calculating the microwave brightness temperature of the ocean surface.

In the discussion of deficiencies we will note some limitation of the particular surface model employed. In addition we will point out certain areas wherefurther experimental or theoretical research could greatly enhance the results from this model.

The merit of our particular approach rests primarily in the ease with which a variety of complicated models can be brought together to model complex situations so often encountered in remote sensing. In addition the mathematical simplicity of this approach facilitates a physical understanding which is often hindered by more involved deductive approaches. We will show in the discussion to follow, how the two factors mentioned directly above, facilitate the investigation of the physics of the increase in microwave brightness temperature with increasing rms wave slope.

LIMITATIONS OF THE COMPOSITE SURFACE MODEL

Although the composite model postulated here for the surface of the ocean seems to be an improvement over previous models, at least three objections can be brought against the validity of the model: 1) The randomly oriented specular facet approximation for the clear water portion of the ocean surface may not characterize surface emission and reflection from those parts of the ocean surface covered by capillary waves whose radii of curvature are less than the wavelength of the emitted and reflected radiation. 2) Multiple surface reflections are ignored. 3) The composite model supposes that the total radiation from the clear water portions and the white water portions of the surface is the sum of the radiation from the individual portions. This model will diverge from reality in case a large percentage of adjacent white water and clear water portions of the surface have dimensions less than the wavelength of the reflected and emitted radiation.

A quantitative theoretical assessment of the magnitudes of items 1) and 3) is a difficult task. While the deviation of the Kirchoff approximation from a more sophisticated model could be assessed theoretically, the percentage of the ocean surface which would violate such a approximation is, to our knowledge, unknown. As for item 3), photographs of the ocean surface (see Pierson (1966)) show for wind speeds less than 20 m/sec. white water and clear water to exist in patches large compared to microwave wavelengths. Above 20 m/sec. white water streaking could affect the validity of assumption 3). More investigation into this matter is needed.

Item 2) should be important only to the radiometric sensing of high sea states at large nadir look angles. If, however, a user application of this nature is uncovered, the model could be altered to include the effects of multiple surface scattering.

LIMITATIONS OF THE SUBMODELS

In addition to the surface model, five other models are used to calculate the apparent temperature of the sea. These are 1) percent white water coverage with wind speed 2) white water optical properties model 3) distribution of the wave slopes, 4) atmospheric radiation model and 5) dielectric constant of sea water. In this section we will discuss extensions for models 1) through 4) which could greatly enhance the accuracy of the total model presented here and would certainly increase the reliability of the remote sensing of wind speeds over the world's oceans.

Percent White Water Coverage Versus Wind Speed

The percent white water coverage as discussed by Cardone (1969) is not a function of the wind speed alone. In addition to the wind speed, foam coverage depends to a large extent upon the state of the wind swept sea surface. Further investigations of the influence on foam coverage by time

varying winds, fetch, depth of water, etc., would increase the reliability of remotely sensing wind speeds.

White Water Optical Properties

The optical properties of sea foam are known to depend on at least three things: 1) Thickness of the foam. 2) Volumetric ratio of air to water in the foam. 3) The incidence angle at which the foam is viewed. Although Droppleman (1970) and Williams (1971) have investigated these effects, more research is justifiable.

Droppleman's investigation into this matter was a theoretical one. The model chosen by him is highly idealized; so it is quite possible that certain optical properties of foam may not be in accordance with Droppleman's predictions.

While the experimental work done by Williams corroborates some of Droppleman's results, a more complete investigation, both in the laboratory and in the field would be a valuable undertaking. Laboratory efforts could establish the effects discussed in the opening paragraph of this section on white water optical properties. Field radiometer measurements could further verify these results.

In addition, the actual configuration of white water on the ocean surface should certainly be established. This configuration could be defined by the statistical distributions of white water thickness, volumetric air to water ratios and surface slopes.

Distribution of the Wave Slopes

Hollinger (1971) has questioned the validity at microwave frequencies of Cox and Munk's optically determined sea slope distribution. He further suggests that this distribution could be seen differently by each microwave frequency and thus explain the dependence of wind sensitivity on frequency. As we will show momentarily, the frequency dependency of wind sensitivity is also a result of the variation of sky temperature with frequency, but as yet Hollinger's suggestion can not be dismissed.

An investigation into this question, using the model developed here, is in progress at NASA/MSC. It is possible that the individual effects of the variation of sky temperature and slope distribution with frequency on wind sensitivity can not be separated without considerable experimental effort.

Atmospheric Radiation Model

The major limitation of the atmospheric model used here is its inability to account for the effects of liquid water in the atmosphere. Such a capability is essential since the radiometric sensing of wind speeds through cloud cover is a most useful application.

Paris (1971) has developed a model to account for such effects, but this model requires as an input, the drop size and spatial distribution of water droplets in the atmosphere. As far as we know, no technique exists which can acquire such data on the scale needed for this application.

Another approach to this problem is multi-frequency sensing which might possibly be used to determine in situ the effects of clouds on the brightness temperature. A theoretical investigation of this possibility, using the model developed here, is in progress here at MSC.

MERITS OF THE NUMERICAL APPROACH

The prime consideration for choosing the numerical model above a more analytical approach to ocean surface modeling, is the ease with which existing submodels may be removed from the computer program circuit (see logic flow chart, Figure 4) and more sophisticated models plugged back in. As an unexpected benefit, we found this approach could be used to further the understanding of the basic physics involved in the wind sensitivity frequency dependence. In this section, the above statements will be discussed in more detail.

In Figure 4 each of the boxes to the right or left of center represent subroutines called within the main program. Thus, when new models for sea foam coverage, etc, become available, the models can be programmed and easily incorporated into the total model.

The main program itself consists of input and output routines, random number generators, geometry logic and iteration logic. Each of these routines are independent of the subroutines and will need no modification to incorporate more sophisticated models.

The iteration logic, shown in the small box in the lower left hand side of Figure 4, is an important portion of the main program. Essentially, this logic keeps track of the location of a solid angle element relative to the entire gain pattern and its position with respect to the atmosphere and surface. The program thus "knows" exactly which point of the surface and atmosphere is being viewed by a particular part of the gain pattern.

The iteration logic thus allows the consideration of a horizontally inhomogenous surface or atmosphere provided the model subroutines are capable of providing data of this nature. Such a feature allows us to consider, for example, surface distributions of white water which are not random. Therefore, if the distribution of surface foam can be specified, (for example,

by a camera boresighted with the radiometer) and this data reduced for input into the main program, then the actual surface can be modeled. In this way, horizontal inhomogeneities in surface temperature and salinity could also be modeled.

The ability to substitute atmospheric models within the program allows a very important point to be proved. Using this method we can show that a variation of sky temperature with zenith angle is necessary to produce the wind sensitivity of the horizontally polarized brightness temperature. Further, the variation of the sky temperature with frequency is sufficient to produce a change in wind sensitivity with frequency.

Figure 9 is a plot of brightness temperature versus nadir look angle calculated for an atmospheric model whose temperature does not vary with zenith angle. We accomplished this simply by disabling the normal atmospheric subroutine and substituting a constant sky temperature of 30° K. 30° K was chosen from Figure 10 as an average temperature of the sky at 19.35 GHz.

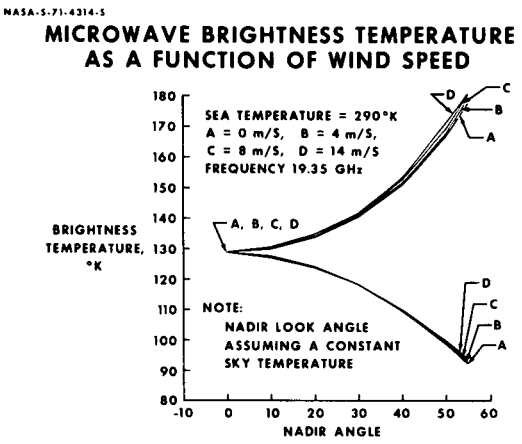

Figure 9.- Brightness temperature versus nadir angle assuming a constant sky temperature of 30° K.

Comparing Figure 9 to Figure 5, we see that the constant sky temperature model completely eliminates the horizontally polarized wind sensitivity. No effect on the vertically polarized component is observed.

We believe the horizontally polarized wind sensitivity is a result of the combined effects of the rms wave slope increase with wind speed and the sky temperature increase with zenith angle. As more and more of the wave

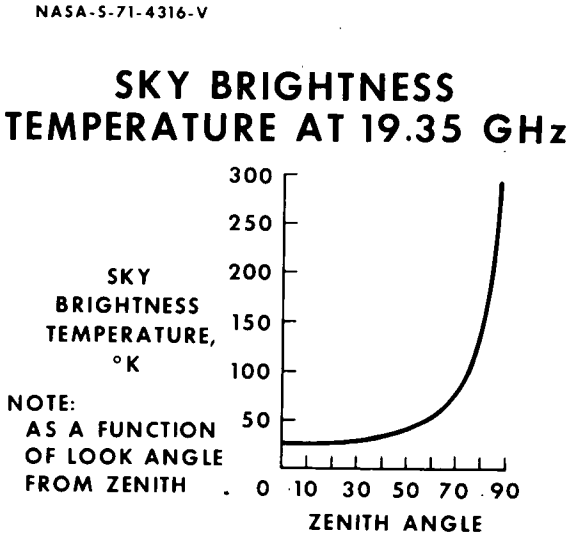

Figure 10.- Sky brightness temperature versus zenith angle for 19.35 GHz.

slopes are oriented toward the horizon by the wind, a hotter portion of the sky is reflected into the radiometer, thus the brightness temperature increases with wind speed. It is believed that the difference in wind sensitivity between the horizontally and vertically polarized brightness temperatures is a result of the difference in the Fresnel reflectivities of a specular facet as shown in Figure 11.

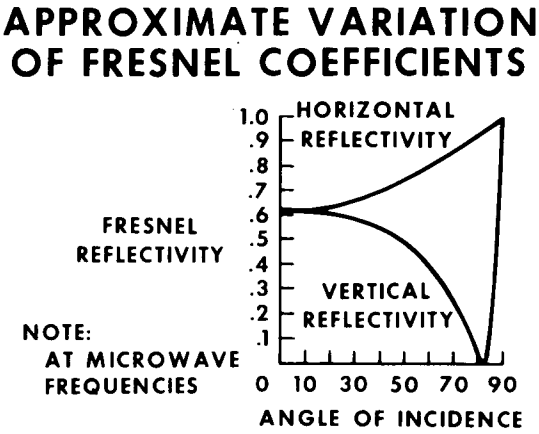

Figure 11.- Approximation variation of Fresnel reflectivities with angle of incidence at 19.35 GHz.

Exactly how the Fresnel coefficients effect this difference is a complex process since for a given facet each polarization mode of the antenna sees the linear combination of the Fresnel coefficients given by equations (4) and (5).

CONCLUSIONS

1. We have developed a mathematical model for the apparent temperature of the sea at all microwave frequencies. The model is a numerical model in which both the clear water wave structure and white water is accounted for as a function of wind speed.

2. This model produces results similar to Stogryn's model at 19.35 GHz for wind speeds less than 8 m/sec. Above 8 m/sec, our model diverges from Stogryn's model which does not include the effects of white water.

3. The model developed here can use radiosonde data to calculate atmospheric effects and can incorporate an empirically determined antenna gain pattern.

4. The computer program is of a modular design. Subroutines called are Cardone's foam coverage vs. wind speed model, Cox and Munk's sea slope distribution model, Droppleman's foam emissivity model, Paris' sea water dielectric constant and atmospheric model. These models can be easily substituted for by other models provided they are coded for the Univac 1108.

5. The computer logic of the main program is capable of treating a horizontally inhomogeneous surface or atmosphere.

6. Computer computation using this model showsthat a variation of microwave sky brightness temperature with zenith angle is <u>necessary</u> to produce the wind sensitivity of the horizontally polarized brightness temperature. The variation of the sky temperature with frequency is <u>sufficient</u> to produce a frequency dependent wind sensitivity.

BIBLIOGRAPHY

1. R.K. Moore and W.J. Pierson, "Worldwide Oceanic Wind and Wave Predictions Using a Satellite Radar Radiometer", AIAA Paper no. 70-310, Presented in Annapolis Maryland, March 1970.

2. J.C. Aukland, P.J. Caruso and W.H. Conway, "Remote Sensing of the Sea Conditions with Microwave Radiometer Systems", AIAA Paper no. 70-318, Presented in Annapolis, Maryland, March 1970.

3. W.H. Peake, "Interaction of Electromagnetic Waves with Some Natural Surfaces", IRE Trans. on Antennas and Propogation, Vol. AP-7, pp. S324-S329, December 1959.

4. A. Stogryn, "The Apparent Temperature of the Sea at Microwave Frequencies", IEEE Trans. on Antennas and Propogation, Vol. AP-15, no. 2, March 1967.

5. G.F. Williams, "Microwave Measurements of Bubbles and Foam", Publisher not located, Univ. Miami, Coral Gables Fla. 33124.

6. J.D. Droppleman, "Apparent Microwave Emissivity of Sea Foam", J. Geophys. Res., Vol. 75, no.3, January 1970.

7. W. Nordberg, J. Conway, Duncan B. Ross, T. Wilheit, "Measurements of Microwave Emission from a Foam Covered, Wind Driven Sea", NASA Preprint X-650-70-384, Oct. 1970 (Submitted for publication to Journal Atmospheric Sciences).

8. James P. Hollinger, "Passive Microwave Measurements of Sea Surface Roughness", IEEE Trans. on Geoscience Electronics, Vol. GE9, no. 3, pp. 165-169, July 1971.

9. Duncan B. Ross, V.J. Cardone and J.W. Conway, "Laser and Microwave Observations of Sea Surface Condition for Fetch-Limited 17-to 25-m/sec. Winds", IEEE Trans. on Geoscience Electronics, Vol. GE 8, no. 4, pp. 326-336, Oct. 1970.

10. J.F. Paris, "Transfer of Thermal Microwaves in the Atmosphere", NASA NGR-44-001-98, Vol. 1, Texas A and M Univ., May 1971.

11. C.Cox and W. Munk, "Measurement of the Roughness of the Sea Surface from Photographs of the Sun's Glitter", J. Opt. Soc. Am., Vol. 44, no. 11, Nov. 1954.

12. J.F. Paris, "Microwave Radiometry and its Application to Marine Meteorology and Oceanography", ONR Contract Nonr 2119 (04), Texas A and M Univ., Jan. 1969.

13. G. Neumann and W.J. Pierson, "Principles of Physical Oceanography", Prentice-Hall, Inc., Englewood Cliffs, N.J., pp.327-329, 1966.

14. D.C. Blanchard "The Electrification of the Atmosphere by Particles From Bubbles in the Sea", Progr. Oceanog., Vol 1, pp. 71-202, 1963.